

# Real-time Raman system for *in vivo* disease diagnosis

Jason T. Motz  
Saumil J. Gandhi  
Obrad R. Scepanovic  
Abigail S. Haka  
John R. Kramer  
Ramachandra R. Dasari  
Michael S. Feld

Massachusetts Institute of Technology  
George R. Harrison Spectroscopy Laboratory  
Cambridge, Massachusetts 02138

**Abstract.** Raman spectroscopy has been well established as a powerful *in vitro* method for studying biological tissue and diagnosing disease. The recent development of efficient, high-throughput, low-background optical fiber Raman probes provides, for the first time, the opportunity to obtain real-time performance in the clinic. We present an instrument for *in vivo* tissue analysis which is capable of collecting and processing Raman spectra in less than 2 s. This is the first demonstration that data acquisition, analysis, and diagnostics can be performed in clinically relevant times. The instrument is designed to work with the new Raman probes and includes custom written LabVIEW and Matlab programs to provide accurate spectral calibration, analysis, and diagnosis along with important safety features related to laser exposure. The real-time capabilities of the system were demonstrated *in vivo* during femoral bypass and breast lumpectomy surgeries. Such a system will greatly facilitate the adoption of Raman spectroscopy into clinical research and practice. © 2005 Society of Photo-Optical Instrumentation Engineers. [DOI: 10.1117/1.1920247]

Keywords: *in vivo* Raman spectroscopy; real-time diagnosis; atherosclerosis; breast cancer; Raman probes.

Paper SS04173RR received Aug. 31, 2004; revised manuscript received Mar. 8, 2005; accepted for publication Mar. 10, 2005; published online May 24, 2005.

## 1 Introduction

Raman spectroscopy is a promising means of studying biological tissue.<sup>1,2</sup> The technique relies on extracting chemical information from a sample based on its molecule-specific Raman emission spectrum, which results from molecular vibrations excited by incident monochromatic light. Up to now, most research in this field has studied excised and cadaveric tissue samples.<sup>3–6</sup> These reports include the examination of atherosclerosis,<sup>3,4</sup> the measurement of blood analytes,<sup>7</sup> and detection of dysplasia and cancer in various tissues including breast,<sup>8–10</sup> cervix,<sup>1</sup> and prostate.<sup>11</sup> Clinical applications have been limited in scope, primarily due to the lack of optical fiber probes capable of effectively acquiring Raman spectra from tissue within the body. As a result, the majority of *in vivo* Raman spectroscopy research has been confined to easily accessible organs and tissues such as skin<sup>12–14</sup> and the cervix.<sup>15</sup>

In order to monitor tissue sites within the body, flexible, small diameter optical fibers must be used to deliver light to the tissue and collect the returning light. Because the probability of Raman scattering is so small, unique challenges must be considered in the design of Raman probes. In particular, two problems must be addressed. First, intense luminescence background generated by the strong monochromatic excitation beam in the delivery and collection optical fibers can mask the signal of interest and generate significant levels of shot noise that compromises the tissue Raman signal. Second,

the probe must be capable of efficient, high-throughput collection, an essential requirement for rapid data acquisition.

Previous Raman studies examining internal body tissues with flexible optical fiber probes have required long collection times, in the range of 5–30 s, which are impractical for many clinical applications.<sup>16–18</sup> Recent advances in probe design in our laboratory have resulted in a flexible Raman probe capable of collecting spectra with large signal-to-noise ratio in 1 s or less.<sup>19</sup> *In vivo* Raman spectroscopy of human arteries<sup>20</sup> and breast tissues has been demonstrated.

Practical implementation of Raman spectroscopy, however, requires an integrated instrument that can provide real-time spectral analysis and diagnostic information to the clinician. A previously described Raman system served as proof of principle for these concepts.<sup>21</sup> Using a commercially available probe to take spectra from a human finger, arm, nail, tooth, and tongue with acquisition times of 5 s, custom-built software was able to provide accurate classification of the different tissue types within 1 s after acquisition.

In this paper we present a real-time Raman instrument with which spectra are acquired in 1 s, while analysis and diagnostic information are provided within an additional second. The instrument is designed to work in conjunction with the newly developed optical fiber Raman probes and its performance is illustrated with data from recent clinical studies of atherosclerosis and breast cancer. The ability to rapidly collect Raman diagnostic information, such as morphological and chemical composition,<sup>3,4,22,23</sup> and provide immediate feedback to the physician during a clinical procedure has the potential to greatly improve patient care by facilitating real-time disease

Address all correspondence to Jason T. Motz., Wellman Center for Photomedicine, Massachusetts General Hospital, Harvard Medical School, 50 Blossom St., BAR704, Boston, MA 02114. Tel: 617-724-3020; Fax: 617-726-4103. E-mail: jmotz@partners.org

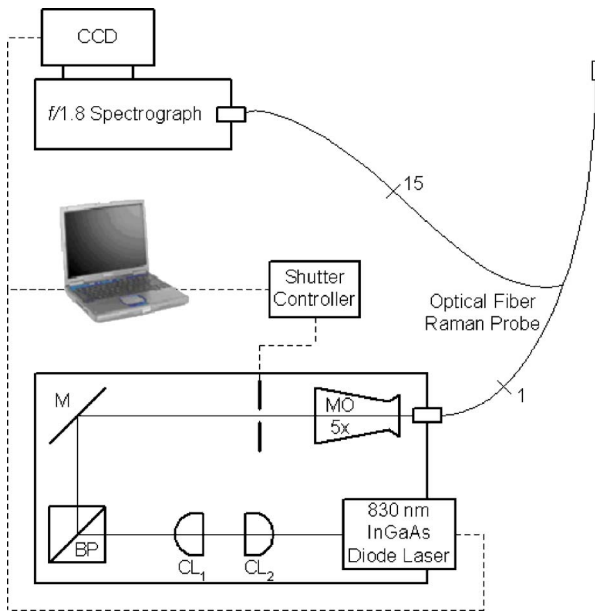


**Fig. 1** Schematic diagram of the clinical Raman system (CL: cylindrical lens; BP: 830 nm bandpass filter; M: mirror; MO: microscope objective; CCD: charge coupled device detector).

management, improving diagnostic accuracy, and allowing early disease diagnosis and long-term monitoring of therapy.

## 2 Instrumentation

The excitation source and detection unit of the clinical Raman system used in this study (Fig. 1) is similar to that described by Brennan et al.<sup>24</sup> and Shim and Wilson.<sup>25</sup> Light from an 830 nm InGaAs diode laser (Process Instruments, Salt Lake City, UT) is collimated by a pair of cylindrical lenses and passed through a holographic bandpass filter centered at 830 nm (Kaiser Optical Systems, Ann Arbor, MI). The light is then coupled into the 200  $\mu\text{m}$  core diameter excitation fiber of the Raman probe using a 5 $\times$  microscope objective (numerical aperture (NA)=0.1, Newport Corporation, Irvine, CA). Illumination of the sample is gated by a high-speed, 6 mm aperture, computer-controlled shutter (LS6ZM2, Vincent Associates, Rochester, NY). The proximal end of the excitation fiber is terminated with an FC connector to provide day-to-day reproducibility of alignment.

A bifurcated optical fiber catheter is used to transport the excitation and Raman scattered light to and from the tissue sample at the distal end of the catheter.<sup>19</sup> Fifteen collection fibers, each with a 200  $\mu\text{m}$  core diameter, surround a single excitation fiber at the distal end of the probe. A short pass filter is placed at the tip of the excitation fiber such that the fiber background is rejected and only 830 nm excitation laser light reaches the tissue. In addition, a long pass filter is placed

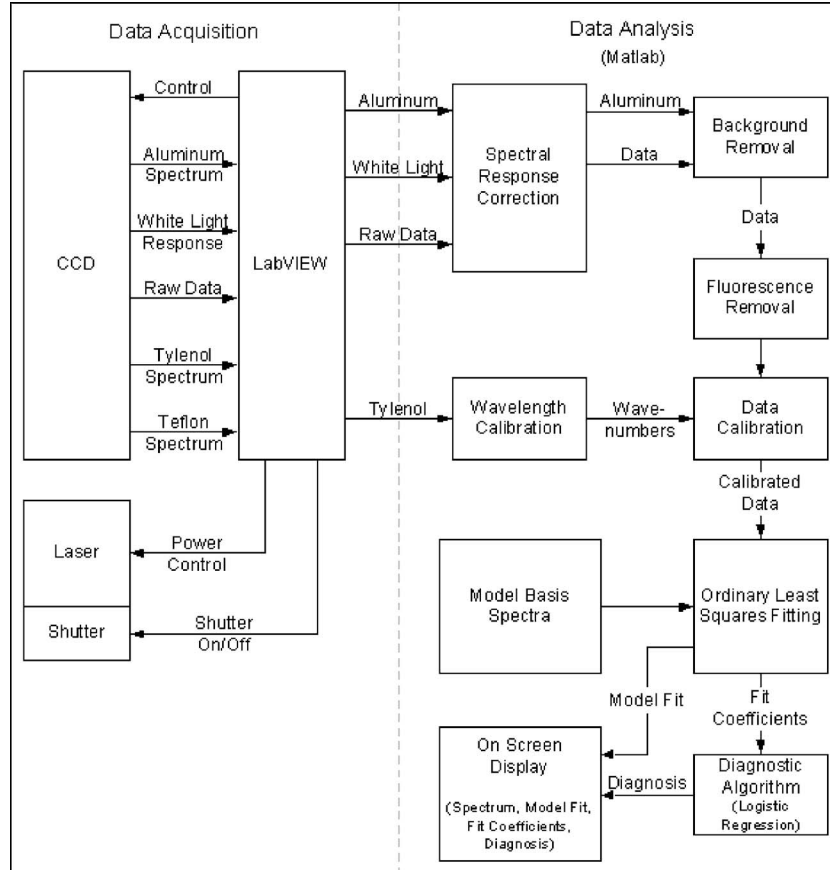


**Fig. 2** Schematic depiction of data flow and interaction of the real-time software with the clinical Raman system.

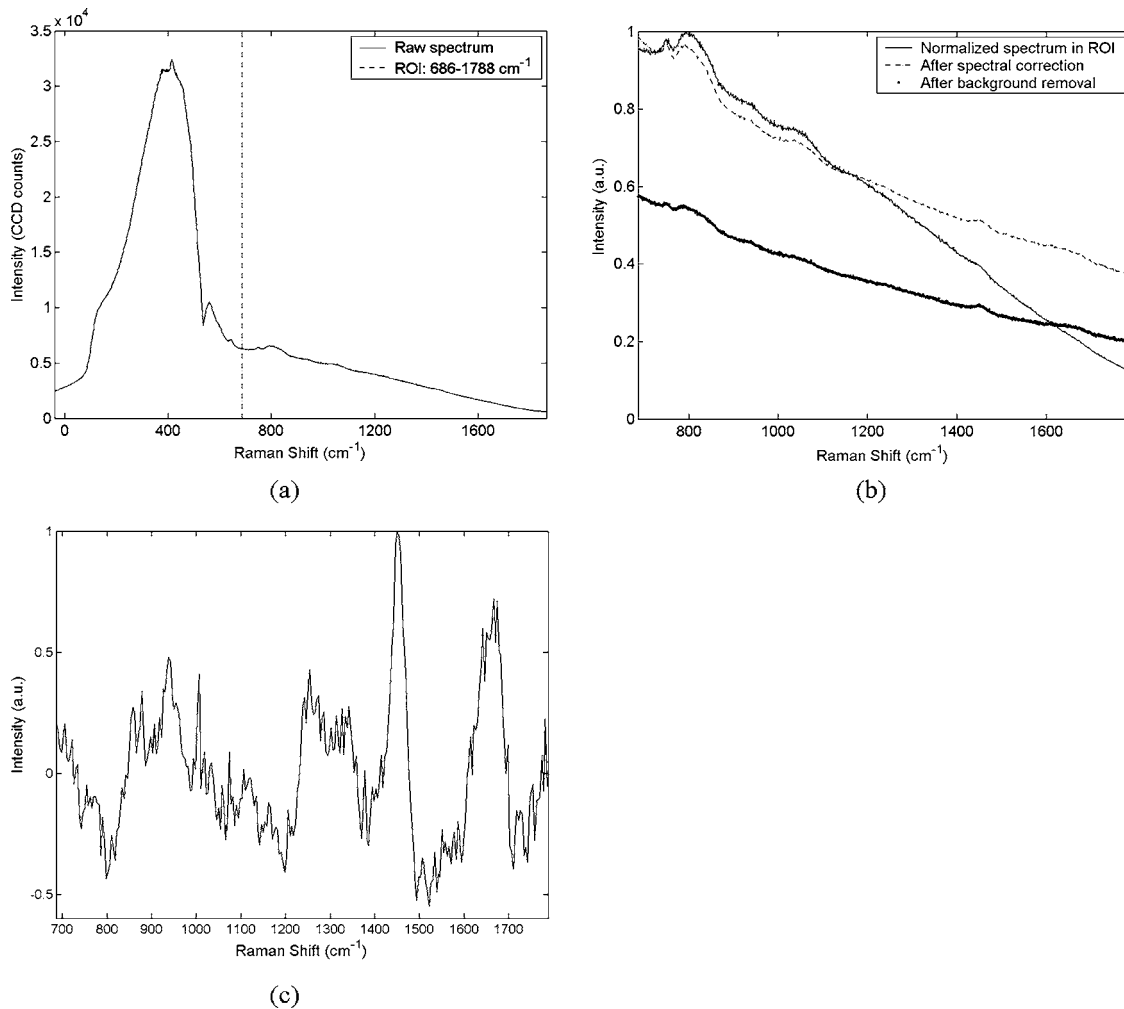


**Fig. 3** *In vitro* Raman spectrum of a non-atherosclerotic femoral artery (a) unprocessed and indicating the biological Raman ROI, (b) after spectral response correction and fiber background removal, and (c) following tissue luminescence removal.

at the tips of the collection fibers in order to minimize the Rayleigh scattered excitation light entering the collection fibers, thereby reducing the generation of additional fiber background. The distal end of the probe is terminated with a sapphire ball lens to enhance signal collection and provide a roughly collimated 200  $\mu\text{m}$  diameter illumination spot. For 100 mW of excitation power, the resultant irradiance is 318  $\text{W}/\text{cm}^2$ . Similar and larger power densities have been used in prior studies and shown to not cause a significant increase in temperature or any damage to arterial tissue.<sup>26,27</sup>

At the proximal end of the probe, the 15 collection fibers are aligned in a linear array, effectively serving as an entrance slit to the spectrograph, resulting in a  $9.4 \text{ cm}^{-1}$  spectral resolution. The fibers are encased in a modified BNC connector to ensure highly reproducible alignment with the connector plate of the spectrograph. Any spectral changes incurred by disconnecting and reconnecting the linear array are below the system's spectral resolution. The numerical aperture of the collection fibers is  $f/\#$ -matched to the HoloSpec  $f/1.8$  spectrograph (Kaiser Optical Systems) to conserve throughput. The spectrograph contains an 830 nm notch filter that further suppresses the elastically scattered Rayleigh light and a holographic grating to disperse the Raman scattered light onto a

back-illuminated, deep-depletion charge coupled device (CCD) detector with a  $1340 \times 400$  array of pixels (Spec-10:400BR, Princeton Instruments, Trenton, NJ). The CCD detector has a 16 bit dynamic range and was liquid nitrogen cooled to  $-110 \text{ }^\circ\text{C}$ . Spectra are obtained by vertically binning the signal from the 15 collection fibers.

### 3 Real-Time Software

The system utilizes LabVIEW software (v 6.1, National Instruments, Austin, TX) as the primary platform to interface with various hardware components of the system and control data flow, allowing automation of more complicated calibration and analysis routines. These subroutines are accomplished *via* a direct interface with Matlab (v.6.5.0, The Mathworks, Natick, MA) and provide relevant diagnostic parameters, such as percentage content of calcification and total cholesterol in the case of atherosclerosis, or collagen and fat in the case of breast cancer.<sup>3,4,22,23</sup> The modular design of the real-time software allows for easy adaptation of the instrument for different applications.

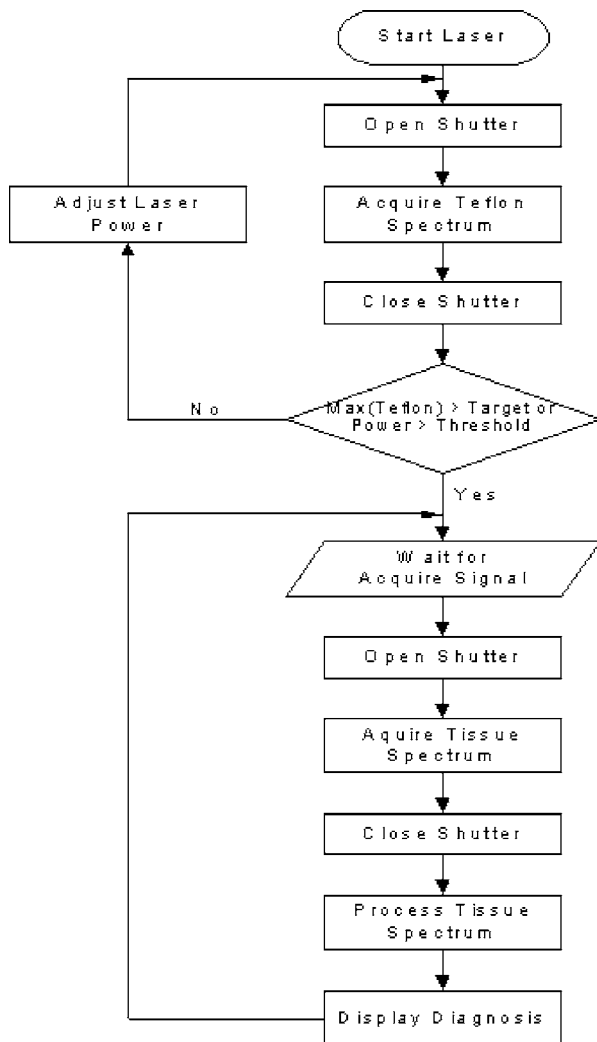


Fig. 4 Real-time data acquisition process.

### 3.1 System Calibration

In order to provide real-time data analysis and diagnosis, spectra for calibration and background subtraction must be acquired prior to data collection. In this study 4-acetamidophenol (Tylenol) was used to calibrate the Raman shift axis. The remaining fiber background signal from the optical fiber probe is characterized by acquisition of a spectrum from roughened aluminum. The spectral response of the collection system is obtained by recording the spectrum of a calibrated tungsten white-light source, diffusely scattered by a reflectance standard ( $\text{BaSO}_4$ ). All calibration spectra are acquired with the same probe to be used for the subsequent procedure and loaded into the system prior to *in vivo* data collection. Alignment and calibration data can all be obtained within a couple of minutes. Following collection of the calibration spectra, the Raman probe is submitted for sterilization. The system has been designed so that it is stable from day to day, thus disconnecting and reconnecting the probe to the system does not change the calibration parameters.

### 3.2 Data Acquisition and Analysis

Figure 2 shows the flow of data between different modules of the real-time software and the clinical Raman system. Lab-

VIEW control of the CCD detector is accomplished through a data acquisition (DAQ) card (PCI-6035E, National Instruments, Austin, TX) with drivers written by R<sup>3</sup>-Software (Lawrenceville, NJ). The right-hand side of Fig. 2 depicts the LabVIEW-Matlab interface for real-time data analysis and disease diagnosis.

A sequence of steps is executed before a Raman diagnosis is extracted from the raw spectrum acquired on the CCD. First, the data are corrected for the system spectral response by dividing them by the white-light spectrum. The resultant data are then normalized to maximum peak height and truncated to the biological Raman region of interest (ROI) appropriate to the models used in this study ( $686\text{--}1788\text{ cm}^{-1}$ ). The next step is to remove the fiber background from the tissue data by subtracting the spectrum acquired from roughened aluminum. The relationship between the intensity of spectra from the aluminum and the tissue spectrum is dependent upon the tissue's optical properties, which are unknown *a priori*. Therefore, we iteratively subtract the same aluminum spectrum scaled by a range of different intensities to determine the optimal ratio for background removal. The spectrum that results in the lowest standard deviation of the residual between the data and the model fit is used for analysis. After fiber background removal, the remaining broadband tissue luminescence is removed by subtracting a sixth order polynomial that is fit to the data.<sup>19,24</sup> This final correction step results in extraction of the Raman spectrum of the examined site. The resultant spectrum is calibrated to a standard set of wavenumber bins. This spectrum is analyzed with the appropriate disease model by using ordinary least squares (OLS), which provides the relative fit coefficients of the various chemical/morphological components of tissue. Finally, the corresponding classification algorithm is invoked to provide a clinical diagnosis for the region of tissue examined (see **Diagnostic Algorithms**, below).

The outlined sequence of calibration and data pre-processing steps is illustrated in Fig. 3 with an *in vitro* spectrum taken from normal femoral artery. The spectrum was collected in four accumulations of 0.25 s for a total collection time of 1 s with 100 mW excitation laser power incident on the sample. As seen in Fig. 3(a), the raw tissue spectrum consists of small tissue Raman features, which are barely discernible above the fiber background, and large, broad tissue luminescence despite the excellent filtering employed in the probe. Figure 3(b) shows the tissue data after its intensity is normalized and corrected for spectral response. The primary effect of this step is to correct for collection system efficiency and the monotonically decreasing quantum efficiency of the CCD at higher wavenumbers. Figure 3(b) also shows the tissue spectrum after final removal of the remaining fiber background. Finally, Fig. 3(c) presents the Raman spectrum of this normal femoral artery after the broadband tissue luminescence has been removed. For consistency with previous studies, the intensity of the spectrum is normalized after tissue luminescence removal.

### 3.3 Diagnostic Algorithms

The real-time software is configured to allow selection of the appropriate spectral model<sup>3,22</sup> and tissue-specific diagnostic algorithms.<sup>4,23</sup> This currently includes those developed in our laboratory for diagnosis of atherosclerosis and breast cancer.

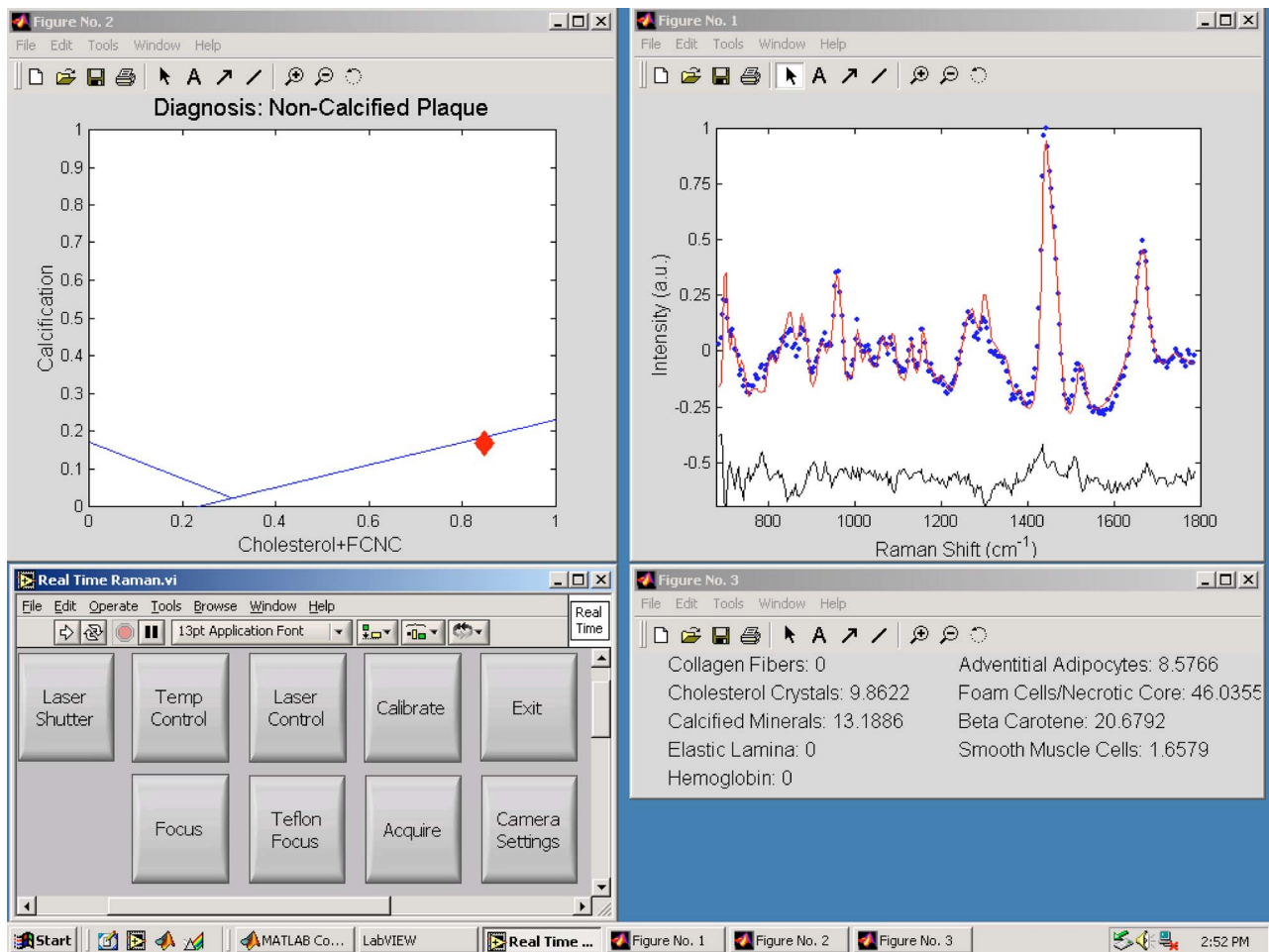


**Fig. 5** Real-time display of tissue Raman spectrum, model fit, residual, fit contributions, and diagnosis of a slightly calcified atherosclerotic plaque sample of femoral artery. The collection time for this *in vitro* spectrum was 1 s with 100 mW excitation power. The total time for data acquisition and analysis was under 2 s.

These models include basis spectra of morphological and chemical components for OLS fitting of the tissue spectra, as well as diagnostic thresholds for disease classification. The user can toggle between the two different models as mandated by the clinical situation. Once the Raman spectrum is extracted, data are fit by OLS using the appropriate user-selected model and the corresponding diagnosis is presented.

### 3.4 Safety

The *in vivo* Raman system must adhere to strict safety guidelines in the clinical environment. Any part of the system that touches the patient directly or indirectly must be kept sterile. Sterilization during this study was performed using cold-gas ethylene oxide. Furthermore, the excitation laser power cannot exceed a predetermined threshold value.

As shown on the left-hand side of Fig. 2, accurate control of the excitation laser power is accomplished with LabVIEW. After sterilization, the probe tip cannot be contaminated by measuring the excitation power with a power meter, therefore we use a sterilized Teflon block to calibrate the excitation laser power. A Teflon spectrum obtained prior to the procedure is used to determine the expected signal (target intensity) for the desired excitation power. During the procedure, spec-

**Table 1** Timing breakdown for data acquisition, analysis, and disease diagnosis necessitated by the clinical Raman system.

Process	Time (ms)
Open laser shutter	0.700
Collection time	1000
Load acquired spectra in Matlab	80
Spectral response correction	1
Fiber background removal	1
Tissue luminescence removal	200
Calibration to standard model bins	480
Ordinary least squares fitting	190
Diagnostic algorithm and on-screen display	70



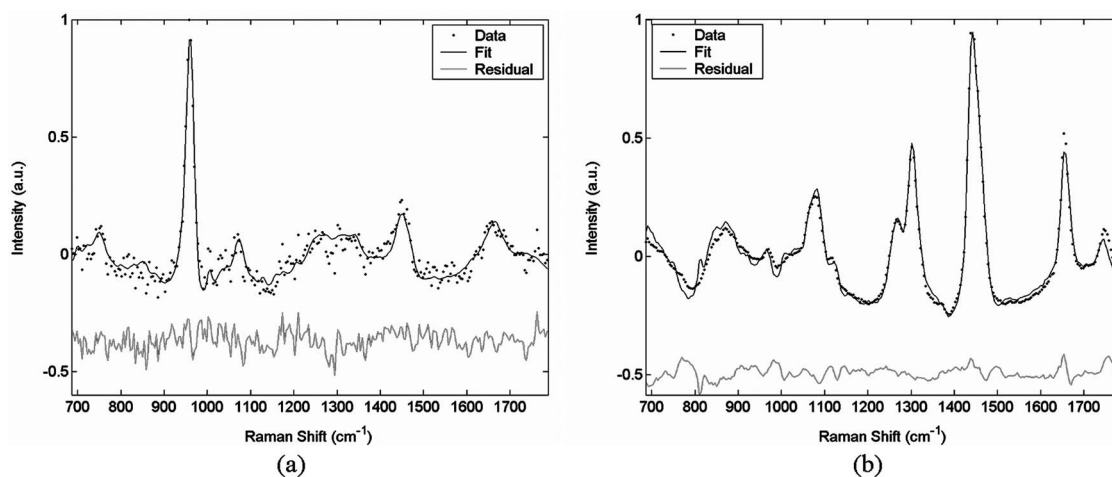


**Fig. 6** Real-time clinical Raman spectra (dots), model fits (lines), and offset residual (data minus fit) of: (a) femoral artery acquired *in vivo* during bypass surgery, and (b) breast tissue acquired *in vivo* during lumpectomy surgery. Both spectra were acquired in 1 s with  $\sim 100$  mW excitation power.

tra of an identical sterilized Teflon block are taken with the same probe used for calibration, and their peak intensities are compared to the target intensity. The laser power is automatically adjusted *via* LabVIEW until the target intensity is obtained, or until a predetermined threshold power is reached (Fig. 4). Laser power is modified remotely with an analog waveform through the DAQ. The alignment procedure takes less than 1 min and typically results in laser powers within 25% of the target.

As a precaution for safety of the operators and patient, the laser beam is gated by a high-speed shutter, also controlled by LabVIEW. The shutter opens automatically just before data acquisition begins and closes immediately after the acquisition is complete. The shutter then remains closed until the system receives a signal through LabVIEW for the next acquisition.

#### 4 System Performance

The tissue Raman spectrum, model fit, residual between the data and model fit, fractional fit coefficients, and diagnosis are plotted on the computer screen (Fig. 5). Using an IBM compatible computer with a clock speed of 2.8 GHz, the entire process of data acquisition, analysis, and diagnosis is accomplished in less than 2 s. The timing breakdown for each step of the process is shown in Table 1.

Limitations to reducing the total time for data acquisition, analysis, and disease diagnosis are mainly imposed by two factors: collection efficiency and data analysis. First, the collection efficiency and throughput of the optical fiber Raman probe determine the time needed for collecting *in vivo* tissue spectra. Significant improvements in the design of the probe filters and collection optics will likely lead to higher throughput and collection efficiency, allowing *in vivo* data acquisition in much less than 1 s.

Reduction in time for data analysis is mainly limited by processor speed. As can be seen in Table 1, the most time consuming steps for data analysis are tissue luminescence removal, data calibration, and OLS fitting of the data. The relationship between the intensity of the aluminum spectrum and

the tissue spectrum is unknown *a priori*. Therefore, the same aluminum spectrum scaled with various intensities is needed to determine the optimal ratio for fiber background removal. As a result, OLS fitting has to be iteratively carried out for each tissue site. Development of algorithms that rely on knowledge of *a priori* probabilities of probing a certain tissue type might further reduce time spent on analyzing the data. In addition, more efficient filtering in future Raman probe designs will further reduce the fiber background and therefore decrease the uncertainty about its magnitude. Calibrating the data to the standard wavenumber bins utilized in the spectral models is the most time consuming step in analysis. It is possible that switching to a more efficient programming platform could provide significant improvements to this performance.

#### 5 Real-Time Diagnosis

We have used the real-time clinical Raman system for *in vivo* studies to diagnose atherosclerosis and vulnerable plaque,<sup>20</sup> and also to provide margin assessment during breast cancer surgery. Data were collected in 1 s with  $\sim 100$  mW excitation power and representative spectra are shown in Fig. 6. All clinical studies were approved by the MIT Committee on the Use Of Humans as Experimental Subjects and the Institutional Review Board of the cooperating hospitals. Informed consent was obtained from all subjects prior to procedures.

#### 6 Conclusion

A Raman spectroscopy system capable of providing real-time disease diagnosis in a clinical setting has been designed, developed, and tested. The implemented software package utilizes LabVIEW to interface with various components in the system. LabVIEW control of system components such as the laser and laser shutter allows data acquisition in accordance with clinical safety guidelines. In addition, we utilize a LabVIEW-Matlab interface to combine the computational power and versatility of both programs to perform real-time data analysis, while maintaining a customizable, user-friendly

interface. The modular design of the system allows easy incorporation of various spectral models. Furthermore, it provides easily adaptable data analysis routines and diagnostic algorithms.

### Acknowledgments

The authors thank Dr. Arnold Miller, Dr. Maryann Fitzmaurice, and Dr. Joseph Crowe for their assistance in clinical procedures and pathological diagnosis. This research was sponsored by the NIH (Grant No. R01-HL-64675) and the National Center for Research Resources program (Grant No. P41-RR-02594). Support was also generously contributed by the Pfizer Corporation and the Lord Foundation of MIT.

### References

- A. Mahadevan-Jansen and R. Richards-Kortum, "Raman spectroscopy for the detection of cancers and precancers," *J. Biomed. Opt.* **1**(1), 31–70 (1996).
- E. B. Hanlon, R. Manoharan, T. W. Koo, K. E. Shafer, J. T. Motz, M. Fitzmaurice, J. R. Kramer, I. Itzkan, R. R. Dasari, and M. S. Feld, "Prospects for *in vivo* Raman spectroscopy," *Phys. Med. Biol.* **45**(2), R1–R59 (2000).
- H. P. Buschman, G. Deinum, J. T. Motz, M. Fitzmaurice, J. R. Kramer, A. van der Laarse, A. V. Brusckke, and M. S. Feld, "Raman microspectroscopy of human coronary atherosclerosis: biochemical assessment of cellular and extracellular morphologic structures *in situ*," *Cardiovasc. Pathol.* **10**(2), 69–82 (2001).
- H. P. Buschman, J. T. Motz, G. Deinum, T. J. Römer, M. Fitzmaurice, J. R. Kramer, A. van der Laarse, A. V. Brusckke, and M. S. Feld, "Diagnosis of human coronary atherosclerosis by morphology-based Raman spectroscopy," *Cardiovasc. Pathol.* **10**(2), 59–68 (2001).
- M. Gniadecka, O. F. Nielsen, D. H. Christensen, and H. C. Wulf, "Structure of water, proteins, and lipids in intact human skin, hair, and nail," *J. Invest. Dermatol.* **110**(4), 393–398 (1998).
- A. S. Haka, K. E. Shafer-Peltier, M. Fitzmaurice, J. Crowe, R. R. Dasari, and M. S. Feld, "Identifying microcalcifications in benign and malignant breast lesions by probing differences in their chemical composition using Raman spectroscopy," *Cancer Res.* **62**(18), 5375–5380 (2002).
- A. M. K. Enejder, T. W. Koo, J. Oh, M. Hunter, S. Sasic, M. S. Feld, and G. L. Horowitz, "Blood analysis by Raman spectroscopy," *Opt. Lett.* **27**(22), 2004–2006 (2002).
- R. R. Alfano, C. H. Liu, W. L. Sha, H. R. Zhu, D. L. Akins, J. Cleary, R. Prudente, and E. Cellmer, "Human breast tissues studied by IR Fourier transform Raman spectroscopy," *Lasers Life Sci.* **4**(1), 23–28 (1991).
- C. J. Frank, R. L. McCreery, and D. C. B. Redd, "Raman spectroscopy of normal and diseased human breast tissues," *Anal. Chem.* **67**(5), 777–783 (1995).
- R. Manoharan, K. Shafer, L. Perelman, J. Wu, K. Chen, G. Deinum, M. Fitzmaurice, J. Myles, J. Crowe, R. R. Dasari, and M. S. Feld, "Raman spectroscopy and fluorescence photon migration for breast cancer diagnosis and imaging," *Photochem. Photobiol.* **67**(1), 15–22 (1998).
- P. Crow, N. Stone, C. A. Kendall, J. S. Uff, J. A. M. Farmer, H. Barr, and M. P. J. Wright, "The use of Raman spectroscopy to identify and grade prostatic adenocarcinoma *in vitro*," *Br. J. Cancer* **89**(1), 106–108 (2003).
- P. J. Caspers, G. W. Lucassen, R. Wolthuis, H. A. Bruining, and G. J. Puppels, "*In vitro* and *in vivo* Raman spectroscopy of human skin," *Biospectroscopy* **4**(5 Suppl), S31–S39 (1998).
- P. J. Caspers, G. W. Lucassen, H. A. Bruining, and G. J. Puppels, "Automated depth-scanning confocal Raman microspectrometer for rapid *in vivo* determination of water concentration profiles in human skin," *J. Raman Spectrosc.* **31**(8–9), 813–818 (2000).
- T. R. Hata, T. A. Scholz, I. V. Ermakov, R. W. McClane, F. Khachik, W. Gellermann, and L. K. Pershing, "Non-invasive Raman spectroscopic detection of carotenoids in human skin," *J. Invest. Dermatol.* **115**(3), 441–448 (2000).
- U. Utzinger, D. L. Heintzelman, A. Mahadevan-Jansen, A. Malpica, M. Follen, and R. Richards-Kortum, "Near-infrared Raman spectroscopy for *in vivo* detection of cervical precancers," *Appl. Spectrosc.* **55**(8), 955–959 (2001).
- H. P. Buschman, E. T. Marple, M. L. Wach, B. Bennett, T. C. Schut, H. A. Bruining, A. V. Brusckke, A. van der Laarse, and G. J. Puppels, "*In vivo* determination of the molecular composition of artery wall by intravascular Raman spectroscopy," *Anal. Chem.* **72**(16), 3771–3775 (2000).
- T. C. Bakker Schut, M. J. H. Witjes, H. J. C. M. Sterenborg, O. C. Speelman, J. L. N. Roodenburg, E. T. Marple, H. A. Bruining, and G. J. Puppels, "*In vivo* detection of dysplastic tissue by Raman spectroscopy," *Anal. Chem.* **72**(24), 6010–6018 (2000).
- M. G. Shim, L. M. Song, N. E. Marcon, and B. C. Wilson, "*In vivo* near-infrared Raman spectroscopy: demonstration of feasibility during clinical gastrointestinal endoscopy," *Photochem. Photobiol.* **72**(1), 146–150 (2000).
- J. T. Motz, M. Hunter, L. H. Galindo, J. A. Gardecki, J. R. Kramer, R. R. Dasari, and M. S. Feld, "Optical fiber probe for biomedical Raman spectroscopy," *Appl. Opt.* **43**(3), 542–554 (2004).
- J. T. Motz, A. Miller, S. J. Gandhi, A. S. Haka, L. H. Galindo, M. Fitzmaurice, R. R. Dasari, J. R. Kramer, and M. S. Feld, "*In vivo* Raman spectral pathology of human atherosclerosis and vulnerable plaque," Submitted (2005).
- T. C. Bakker Schut, R. Wolthuis, P. J. Caspers, and G. J. Puppels, "Real-time tissue characterization on the basis of *in vivo* Raman spectra," *J. Raman Spectrosc.* **33**(7), 580–585 (2002).
- K. E. Shafer-Peltier, A. S. Haka, M. Fitzmaurice, J. Crowe, J. Myles, R. R. Dasari, and M. S. Feld, "Raman microspectroscopic model of human breast tissue: implications for breast cancer diagnosis *in vivo*," *J. Raman Spectrosc.* **33**(7), 552–563 (2002).
- A. S. Haka, K. E. Shafer-Peltier, M. Fitzmaurice, J. Crowe, R. R. Dasari, and M. S. Feld, "Detecting breast cancer using Raman spectroscopy," Submitted (2005).
- J. F. Brennan, Y. Wang, R. R. Dasari, and M. S. Feld, "Near-infrared Raman spectrometer systems for human tissue studies," *Appl. Spectrosc.* **51**(2), 201–208 (1997).
- M. G. Shim and B. C. Wilson, "Development of an *in vivo* Raman spectroscopic system for diagnostic applications," *J. Raman Spectrosc.* **28**(2–3), 131–142 (1997).
- G. J. Puppels, T. C. Bakker Schut, P. J. Caspers, R. Wolthuis, M. van Aken, A. van der Laarse, H. A. Bruining, H. P. J. Buschman, M. G. Shim, and B. C. Wilson, "*In Vivo* Raman Spectroscopy," in *Handbook of Raman Spectroscopy*, I. R. Lewis and H. G. M. Edwards, Eds., pp. 549–574, Dekker, New York (2001).
- J. T. Motz, *Development of in vivo Raman spectroscopy of atherosclerosis*, PhD thesis, Massachusetts Institute of Technology, Cambridge (2003).